

VIBRATION INSTITUTE 33RD ANNUAL MEETING , HARRISBURG , PA . , JUN E 23-2 7, 2009

UNDERSTANDING AMPLITUDE AND PHASE IN ROTATING MACHINERY

Edgar J. Gunter, Ph.D.
Professor Emeritus
Department of Mechanical and Aerospace Engineering
Former Director, Rotor Dynamics Laboratory
University of Virginia
RODYN Vibration Analysis, Inc.
DrGunter@aol.com

Abstract:

The measurement of phase is essential in the balancing of single- or multi-plane balancing of rotating machinery. The rate of change of phase is important, as it may indicate the presence of a critical speed, and from the rate of change of phase one may be able to deduce the amplification factor or log decrement of a particular mode. Having a phase reference mark is particularly critical on complex machinery such as gas turbines and also the space shuttle oxygen and hydrogen pumps. Without the presence of a phase signal, it is impossible to determine what component of the total vibration is synchronous and what is due to external or subsynchronous vibrations. The use of the timing mark, therefore, allows us to track amplitude and phase to determine critical speeds, amplification factors, and balancing.

Keywords: Phase; Bode Plots; Nyquist Plots; Amplification Factor; Critical Speeds; Log Decrement

Introduction:

The understanding of amplitude-phase relationships is extremely important for all users of turbo-machinery, as well as the manufacturers. One of the greatest problems in the diagnosis and correction of field problems with rotating machinery is the lack of adequate vibration instrumentation on the machinery to observe the vibrations, the lack of adequate balancing planes, and most important, the lack of a phase reference signal. The field installation of vibration instrumentation and a phase indication probe are often very difficult and time consuming to achieve. A great deal of time, effort, and efficiency would be achieved if manufacturers had adequately designed the machinery with the idea of sufficient instrumentation, balance planes, and phase reference signal for machine diagnosis and balancing.

For example, without an adequate reference signal it is difficult to separate synchronous from nonsynchronous motion on a turbo-rotor and makes the problem of field balancing extremely difficult. Some notable examples that will be discussed are the correction of the failure problem encountered with the space shuttle main engine oxygen pump. The oxygen pump vibration failure is an example in the extreme of what happens without the application of a suitable reference signal. The vibration of interest in the oxygen pump was initially drowned out by the high intensity, high frequency vibrations generated by the rocket engine. It was only after a reference signal was generated laboriously from the four-lobed speed pickup that the vibration could be suitably analyzed and the pump design corrected. Once the timing mark was secure, synchronous tracking filters showed that the oxygen pump was operating at a second critical speed. The pump seals then could be redesigned to suppress this critical speed in order for the pump to operate safely through the entire speed range. Another notable example was the attempt to analyze the vibration characteristics of a typical commercial small jet aircraft engine. Although years of vibration data had been taken on this engine, it proved to be worthless since there was no corresponding phase reference mark to determine the nature of the critical speeds and the amount of damping in the modes. New data had to be generated, which included a timing reference mark, in order to ascertain the problems. Many field problems in vibration diagnostics and field balancing could be more easily resolved if adequate provisions had been initially made to provide adequate phase measurements.

What is Phase and What Does it Mean?:

The electrical engineers are well acquainted with phase. The phase of two or three voltages such as 3 phase motors is well established and the understanding of phase and power factor is critical in electrical equipment. The roll of phase and its measurements in rotating machinery is not as well established or appreciated by many manufactures.

Phase Measurements With Strobe Light:

One of the earliest methods of phase measurements was the use of a strobe light which was triggered by a velocity pickup. Fig. 1 shows the phase position before and after the placement of a trial weight on a rotor balancing demonstrator.

The phase measurements are made from the stationary compass. The initial strobe light shows the arrow pointing at 270 deg. After placement of the trial weight, the strobe light shows that the phase has shifted 60 deg in the clockwise direction.

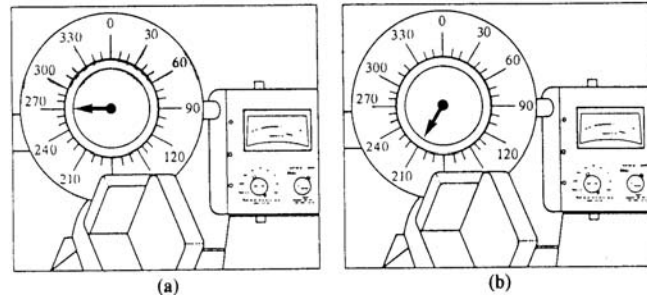


Fig. 1 Phase Readings With 2 gm Trial Weight

Although balancing may be made from such measurements, the strobe light procedure of relative phase measurements provides little insight to the actual rotor dynamics amplitude-phase relationship.

The strobe light is triggered to flash based on the signal received from the analyzer. The strobe light is made to flash on the shaft, freezing it in place. When a strobe light is used for a phase reference in balancing, the determination of the rotor high spot is not as simple or straightforward as when a noncontact probe and a keyphasor reference mark are used.

Fig. 2, developed by C. Jackson, represents the phase angle for a typical seismic vibration analyzer in the displacement mode. In addition to the 90 deg phase shift due to integration of the velocity signal, there is a speed-dependent rolloff phase shift due to the mass inertia effects of the velocity sensor at low frequencies.

Fig 2 was developed by Jackson to help find the rotor heavy spot for assistance in the placement of the initial trial weight for influence coefficient balancing.

Amplitude and Phase Measurements With Noncontact Inductance Probes:

A noncontact probe has the distinct advantage of observing shaft motion directly. One of the earliest types of noncontact displacement probe dating to the 1960's was the British Wayne-Kerr capacitance probe. This probe was ideally suited for early gas bearing rotor dynamic studies but was not practical for industrial rotating equipment. This was due to the cost of the equipment, problems of contamination of the probe surface and limited range of motion.

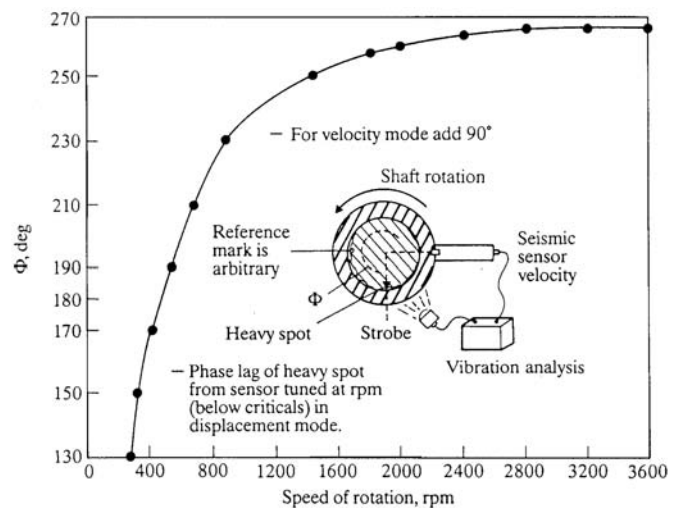


Fig 2 Phase Lag From Seismic Velocity Sensor to Rotor Heavy Spot (Jackson, 1979)

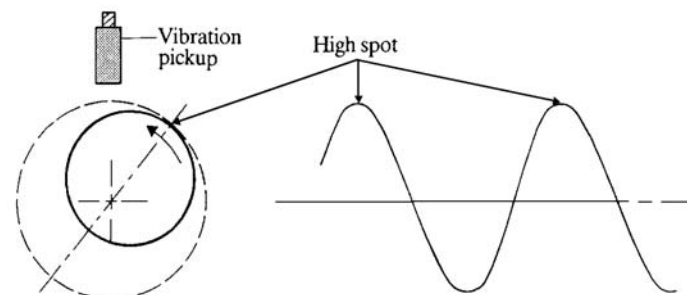


Fig. 3 Shaft Motion With Noncontact Displacement Probe

Fig. 3 represents the direct shaft displacement as observed by a noncontact probe. To view this motion, the vibration signal was displayed on an oscilloscope and the motion recorded by a Polaroid camera. No phase measurements were recorded with this early procedure. By taking a series of pictures at various speeds, a crude plot of amplitude vs speed could be attained.

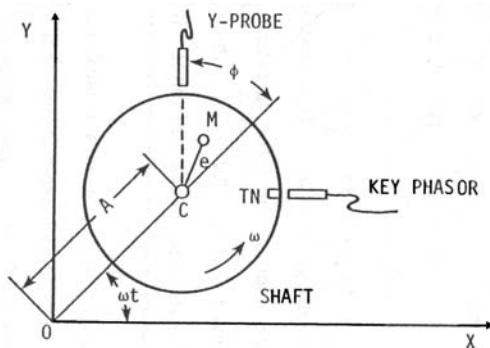


Fig. 4 Noncontact and Keyphasor Probes

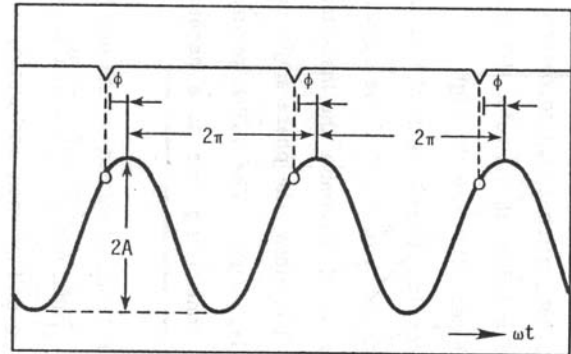


Fig. 5 Amplitude Signal With Keyphasor Mark

A major advancement in the understanding of rotor dynamic amplitude-phase relationships was the introduction of the Bently noncontact inductance vibration pickup. Unlike the Wayne Kerr capacitance probe, the inductance probe was much less expensive, rugged, and with a larger range of motion. A unique innovation of Donald Bently, before the advent of the FFT analyzer, was the introduction of the keyphasor

Fig. 4 represents a typical setup with an inductance probe to monitor shaft motion and the addition of a second probe referred to as the keyphasor probe. A groove is placed on the shaft in line with the keyphasor probe. When the shaft notch passes under the keyphasor probe, a signal is generated as shown in Fig. 5. When the output of the keyphasor is fed into the z-axis of an oscilloscope, a bright spot occurs on the vibration signature as shown in the lower waveform as seen in Fig. 5.

The phase convention, in this case is the angle ϕ , as measured from the bright spot on the wave form of Fig 5 to the peak amplitude. This angle has a practical significance in balancing. For example, if one lines up the timing reference mark with the keyphasor probe, the peak amplitude A occurs at the angle ϕ as measured from the inductance probe in the direction opposite to rotation. This point is often referred to as the “*high spot*”. The location of the unbalance is referred to as the “*heavy spot*”.

If we know the approximate critical speed of the rotor, then we have an idea of where to place the first trial weight for field balancing for a relatively simple rotor system. If the rotor is operating in the subcritical speed range (well below the first critical speed), then the high spot and the heavy spot are in the same vicinity. The first initial trial weight would be placed 180 deg from the high spot. If the rotor was operating well above the first critical speed, for the case of the simple single mass Jeffcott rotor, the mass center is out of phase to the maximum displacement or high spot. In this case the initial trial weight would be placed at the angle ϕ as measured counter rotation from the inductance probe. This placement seems against intuition. If we should attempt the unusual balancing procedure of balancing at the critical speed, then in this case the mass center is leading the mass center by 90 deg. In this case one would line up the keyphasor probe with the notch and place the first trial weight at an angle of $90 + \phi$ deg as measured opposite of rotation from the inductance probe. Such a direct understanding of the relationship between the peak amplitude and the approximate location of the unbalance is not possible with the strobe light method.

Amplitude and Phase Relationships For the Jeffcott Rotor:

The first English publication to describe the dynamics of the flexible single mass rotor was presented by H.H Jeffcott in 1919. He correctly expressed the equations of motion of the single mass rotor with unbalance and damping and presented an explanation of how the rotor could pass successfully through the critical speed. He also showed the displacement-phase relationship at speeds below, at and above the critical speed. To properly understand rotor dynamics amplitude-phase relationships and their implications, we must have a good understanding of the simple Jeffcott rotor.

One of the earliest accounts on rotor dynamics was the article presented in 1869 by W. A Rankine entitled “*On the Centrifugal Force of Rotating Shafts*”, Engineer, Vol 27,London. Rankine introduced the elementary concept of indifferent rotor equilibrium. Rankine examined the equilibrium conditions of a frictionless, uniform shaft disturbed from its initial position. Because he neglected the influence of the Coriolis force, he concluded that: motion is stable below the first critical speed, is neutral or in “indifferent “ equilibrium at the critical speed , and is unstable above the critical speed.

During the next half century, this analysis lead engineers to believe that operation above the first critical speed was not possible. It was not until 1895 that DeLaval demonstrated experimentally that a steam turbine was capable of sustained operation above the first critical speed.

Fig. 6 represents the single mass Jeffcott rotor. In this model the mass is concentrated at the shaft center and the disk is considered as massless. The bearings at taken as simple supports. The damping is applied at the disc center. This assumption may also be considered as a form of model damping. The unbalance in the disk is created by the small offset e_u of the disk center from the axis of rotation.

The equations of motion of the single-mass Jeffcott rotor may be combined into one complex vector equation by means of the complex variable transformation $Z = X + I Y$ as follows:

$$M\ddot{X} + C\dot{X} + KX = M e_u \omega^2 \cos(\omega t) \quad (1)$$

$$M\ddot{Y} + C\dot{Y} + KY = M e_u \omega^2 \sin(\omega t) \quad (2)$$

$$M\ddot{Z} + C\dot{Z} + KZ = M e_u \omega^2 e^{i\omega t} \quad (3)$$

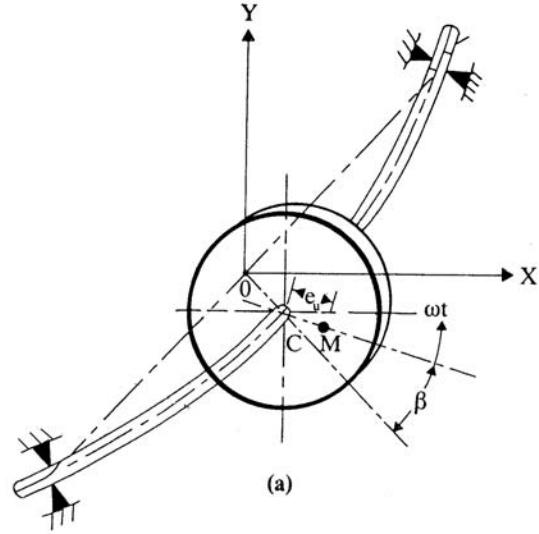


Fig 6 Single Mass Jeffcott Rotor

The steady state synchronous unbalance response due to unbalance is given by:

$$Z_{Steady\ State} = \frac{M e_u \omega^2}{K - M \omega^2 + i C \omega} e^{i(\omega t - \phi_u)}; A = \frac{f^2}{\sqrt{(1 - f^2)^2 + (2\xi f)^2}} e^{i(\omega t - \phi)} \quad (4)$$

The amplitude and phase may be expressed in dimensionless form by using the following variables:

$$\omega_{cr} = \sqrt{\frac{K}{M}} \quad = \text{natural frequency on rigid supports}; \quad \frac{\omega}{\omega_{cr}} = f \quad \text{frequency ratio}$$

$$C_c = 2M\omega_{cr} \quad = \text{critical damping}; \quad \frac{C}{C_c} = \xi \quad \text{damping ratio}; \quad \frac{\delta}{e_u} A = \text{dim amplitude}$$

The relative phase angle lag β of the deflection vector from the rotating unbalance load is given by

$$\beta = \tan^{-1} \frac{2\xi f}{1 - f^2} \quad (5)$$

Amplitude and Phase of the Jeffcott Rotor Below, At and Above The Critical Speed:

There are 3 distinct ranges of motion for the Jeffcott rot In each of these ranges, the phase angles are distinctly different. The first speed range of interest is the speed range referred to as the subcritical speed range.

In this speed range we have the condition that the operating speed is much lower than the critical speed.

Case 1 -Subcritical Speed Operation

Thus we have the condition that $f \ll 1$ and the dimensionless amplitude and phase angle is approximately given by:

$$A = f^2 \quad (6)$$

$$\beta = 0^0 \quad (7)$$

This implies that at low speeds well below the first critical speed, the amplitude of motion due to unbalance excitation is increasing as speed squared. This region is characterized as rigid body motion region. Many current industrial fans are designed to operate in this region as rigid body rotors often with highly undesirables effects. The location of the mass unbalance is in phase with the maximum deflection. In this low speed region, we say that the high spot and the heavy spot coincide

Case 2 - Critical Speed Operation

The second region is a unique region in which the rotor is operating exactly at the critical speed.

In this case $f=1$ and the dimensionless amplitude of motion is given by:

$$A_{f=1} = A_{cr} = \frac{1}{2\xi} \quad (8)$$

The mass center is leading the maximum deflection by:

$$\beta = 90^0 \quad (9)$$

Where A_{cr} is referred to as the critical speed amplification factor on rigid supports. This is a finite value depending upon the modal damping acting upon the rotor. It should be noted that with the Jeffcott rotor all of the damping is concentrated at the disk. The bearings are providing no damping since they are node points.

With a rotor supported on rolling element bearings, the amount of aerodynamic drag damping available at the center disk can be quite small. This could lead to dangerously high levels of vibration if such a rotor were to be continuously under these conditions.

Case 3 - Supercritical Speed Operation

In the supercritical speed the rotor speed is well above the critical speed. This region is referred to as supercritical speed operation in which the dimensionless speed $f \gg 1$. The dimensionless amplitude of motion is given by:

$$A = 1 \quad (10)$$

In this region of operation, the amplitude of motion is no longer increasing as mass center inversion has occurred. The rotor is spinning or rotating about the center of mass. Since the center of mass is offset from the axis of rotation, the inductance probes observe an orbit with radius $e_u...$

The phase angle of motion β is now out of phase to the displacement vector and is given by:

$$\beta = 180^0 \quad (11)$$

Fig. 7 shows the motion of the Jeffcott rotor in the speed ranges.

In the first figure, the speed is well below the critical speed. Point M represents the location of the mass center. Point C is the center of rotation of the shaft. The point H represents the high spot and is in line with the mass center, line C-M extended. At this low speed, the balance correction weight would be placed opposite the high spot. The center figure represents the rotor operating at the critical speed. In this case, the rotor mass center is leading the maximum amplitude or high spot H by 90 deg. If one were to mark the high spot, (as I had once observed in industry on an experimental rotor with caulk), one would place the balance correction at 90deg from the mark opposite the direction of rotation. The third figure on the right represents the shaft motion well above the critical speed. The mass center has inverted 180 deg and is now opposite the high spot .

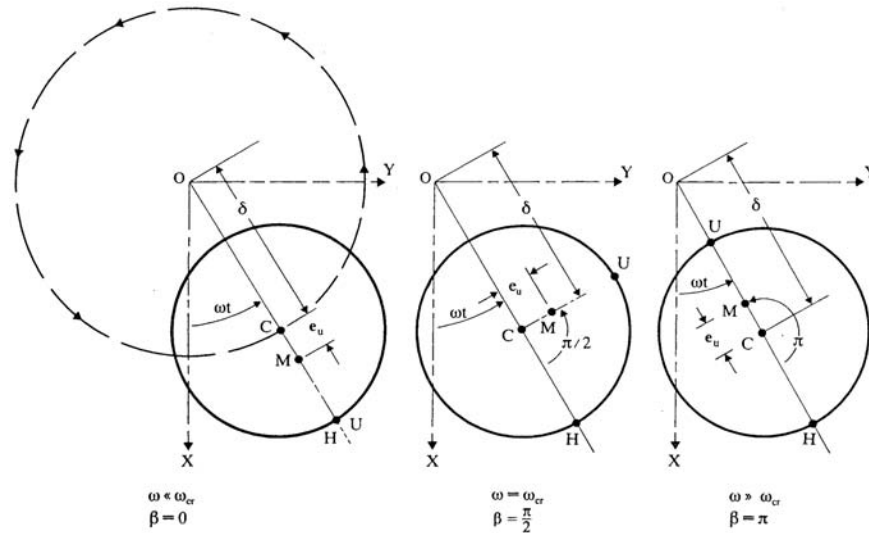


Fig. 7 Jeffcott Rotor Motion Below, At and Above The Critical Speed

Development Of A Jeffcott Rotor Using *DyRoBes* Rotor Dynamics Software:

A single mass rotor model was developed using *DyRoBes* to simulate an idealized Jeffcott rotor. A 200 lb disc was mounted on a steel shaft of 40 inches length with a diameter of 4 inches. To simulate rigid bearings, bearing stiffness values of 1.0e7 Lb/in were assumed. Since the shaft weight is included in this model, the modal weight is the sum of the disk weight W_d plus one-half the shaft weight W_s . The total Jeffcott modal weight then is approximately 271 lb.

Fig. 8 represents the Jeffcott rotor on stiff bearings mounted on a 40 inch shaft.

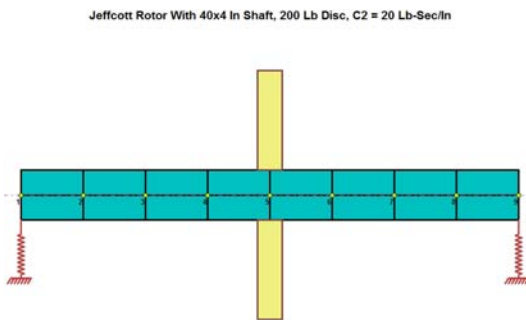


Fig. 8 Jeffcott Rotor on Stiff Bearings

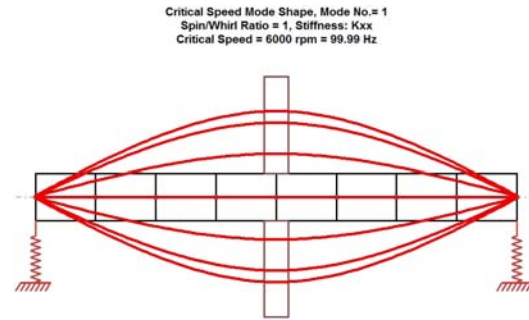


Fig. 9 1st Critical Speed of Jeffcott Rotor at 6,000 RPM

Fig. 9 represents the animated 1st critical speed of the Jeffcott rotor. It should be noted that with the Jeffcott rotor, there is no bearing motion. Anytime this situation occurs in a real rotor one has a dangerous condition in which the bearings will provide no damping. In order to provide damping for the Jeffcott rotor, a third “bearing” was applied acting at the disc center. At this bearing location, damping in both x-y directions of 20 lb-sec/in was assumed.

The critical damping for the Jeffcott rotor is given by:

$$C_c = 2 M \omega_{cr} = 2 \cdot 271 \text{ lb} / 386.4 \times 628 \text{ rad/sec} = 881 \text{ lb-sec/in}$$

For an assumed amplification factor of 20, $\xi = 1/40 = 0.025$

The amount of damping acting at the disk center is given by $C = 0.025 C_c = 22 \text{ lb-sec/in}$

Fig. 10 represents the damped mode shape of the Jeffcott rotor with damping of 20 lb-sec/in added at the disk center. The addition of the damping causes a slight reduction of the damped natural frequency to 5998 RPM. The modal damping is expressed in terms of the log decrement δ .

The relationship between log decrement, ζ ; the damping ratio ξ and critical speed amplification factor is as follows:

$$\delta = \frac{2\pi\xi}{\sqrt{1-\xi^2}} \quad (11)$$

$$A_{cr} = \frac{1}{2\xi} = \frac{\pi}{\delta\sqrt{1-\xi^2}} \approx \frac{\pi}{\delta} \quad (12)$$

Precessional Mode Shape - STABLE FORWARD Precession
 Shaft Rotational Speed = 6000 rpm, Mode No. = 2
 Whirl Speed (Damped Natural Freq.) = 5998 rpm, Log. Decrement = 0.1444

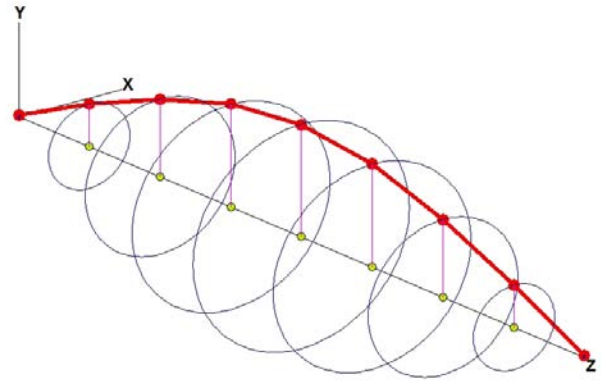


Fig. 10 Damped 1st Mode of Jeffcott Rotor With 20 Lb-Sec/In Damping Applied At Disc

Therefore, for low values of the damping ratio ξ , the critical speed amplification factor A_{cr} is given in terms of log decrement as π/ζ . The log decrement for the 1st forward rotor mode as show in Fig 10 is $A_{cr} = \pi/.144 = 21.8$. This high amplification factor could be expected with a rotor operating on rolling element bearings.

Synchronous Unbalance Response and Phase With Jeffcott Rotor:

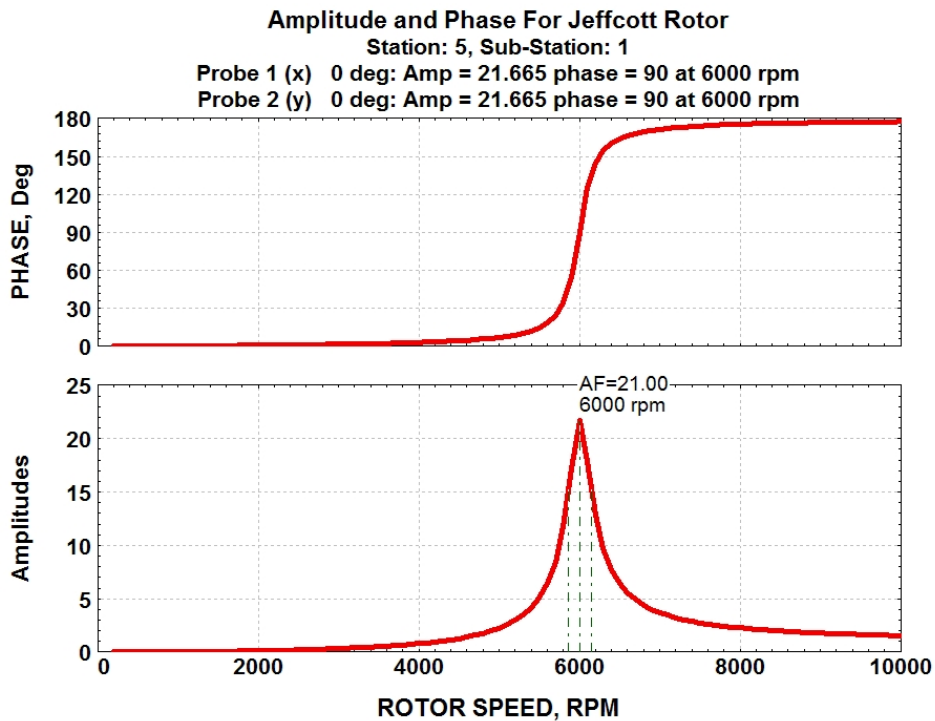


Fig. 11 Synchronous Unbalance Response and Phase of Jeffcott Rotor

Figure 11 represents the unbalance response and phase of motion of the Jeffcott rotor with 2 oz-in of unbalance. The motion is shown for the x probe. The unbalance is assumed to lined up with the keyphasor probe. Here we see the classical 180 deg phase shift with the Jeffcott rotor. The motion plotted is for the center span of the rotor..If a probe were situated at the center span of a multi-mass rotor or large turbine, we would see a similar type of phase shift. Figure 11 represents the typical response observed with the Jeffcott rotor. At speeds below the critical speed, the amplitude increases with speed squared. There is very little shift in phase.

As we approach the critical speed, we see a rapid change in the phase angle. The rate of change of phase is dependent upon the amount of damping present in the rotor system. As we approach speeds well above the critical speed, there is no further change in phase. This is because the mass center has inverted. The rotor spin axis now passes through the rotor mass center. The displacement is now 180 deg out of phase to the mass.

Determination of Amplification Factor From Amplitude and Phase Response:

There are several methods in which the rotor amplification factor may be determined. One of the most common methods taken from electrical engineering is the half power point method. At the critical speed, the speed increment ΔN is measured at a height of $0.707 X_{max}$ at the critical speed. In this case the maximum amplitude at the critical speed is seen from Fig. 11 to be 21.665 mils. Therefore at the height of 0.707×21.666 of 15.3 mils, the band width is measured to be 286 RPM. The critical speed amplification is given by:

$$A_{cr} = \frac{N_{CR}}{\Delta N} = \frac{6,000 \text{ RPM}}{286 \text{ RPM}} = 21 \tag{13}$$

This number agrees well with the computed amplification factor based on the calculation of the log decrement from the damped whirl mode as shown in Fig.10.

A second method used for the determination of the system amplification factor is to determine the rate of change of the phase angle at the critical speed. For example, the greater the measured rate of change of phase while passing through the critical speed, the higher the amplification factor. Mathematically, this is determined by differentiating the rate of the phase angle β (or ϕ) with respect to the dimensionless frequency ratio f . By evaluating this rate of change at the critical speed, given by $f=1$, we obtain the following:

$$\frac{d\beta}{df}_{f=1} = \frac{1}{\xi} = \frac{A_{CR}}{2} \tag{14}$$

This method is often employed with FFT analyzers for the determination of amplification factors.

A third method for determination of the amplification factor from the unbalance response curve is to divide the peak amplitude at the critical speed by the amplitude at speeds well above the critical speed. At high speeds, the rotor amplitude of motion is equal to unbalance eccentricity e_u . Dividing the maximum amplitude by the high speed amplitude yields the critical speed amplification factor as follows:

$$A_{cr} = \frac{A_{max}}{e_u} = \frac{21.64 \text{ mils}}{1 \text{ mil}} = 21.6 \tag{15}$$

Jeffcott Rotor 3 Dimensional Modes at Various Speeds:

Rotor Speed = 4000 rpm, Response - FORWARD Precession
Max Orbit at stn 5, substn 1, with a = 0.00039853, b = 0.00039853

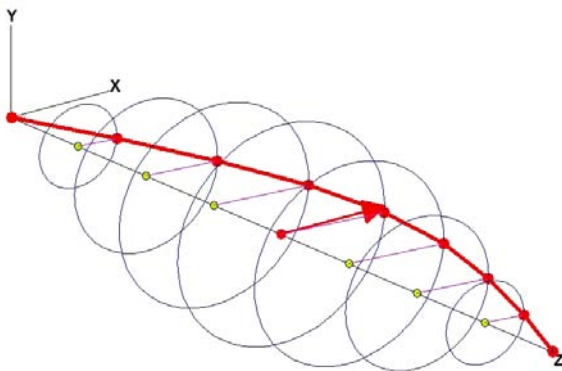


Fig. 12 Jeffcott Rotor Motion at 4,000 RPM

Rotor Speed = 6000 rpm, Response - FORWARD Precession
Max Orbit at stn 5, substn 1, with a = 0.010832, b = 0.010832

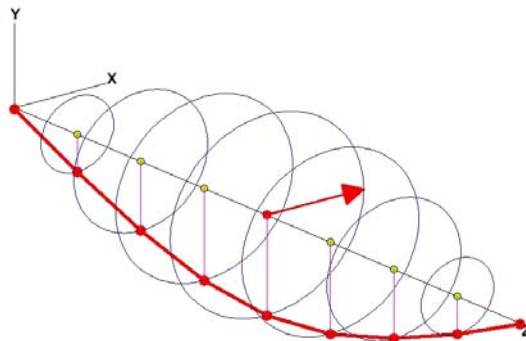


Fig. 13 Jeffcott Rotor Motion at the Critical Speed - 6,000 RPM

Figure 12 represents the 3 dimensional rotor motion at 4,000 RPM which is a speed of two-thirds of the critical speed. It is seen that the unbalance vector and amplitude of motion are essentially in phase.

Figure 13 shows the rotor motion at the critical speed of 6,000 RPM. In this case, the rotating unbalance vector is leading the displacement vector by 90 deg. For slight speed changes either above or below this speed, the phase angles will rapidly change. This makes balancing near the critical speed most difficult.

Figure 14 shows the Jeffcott rotor motion at a speed of 2,000 RPM above the critical speed. Since the rotor system is lightly damped, this increase in speed is sufficient to cause an additional 90 deg shift in phase. We now have a situation in which any further increase in speed will not result in any further increase in either amplitude or phase. The mass center is now fully inverted.

Rotor Speed = 8000 rpm, Response - FORWARD Precession
Max Orbit at stn 5, substn 1, with a = 0.0011345, b = 0.0011345

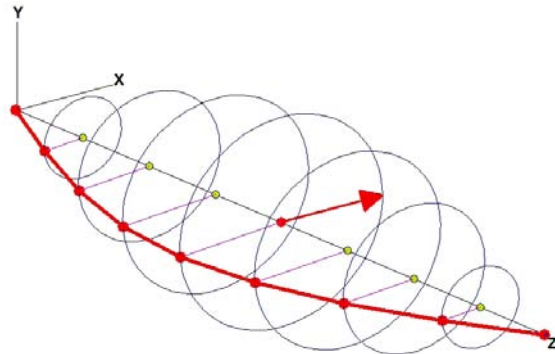


Fig. 14 Jeffcott Rotor Motion Above the Critical
Jeffcott Rotor Polar Plot of Horizontal Shaft Motion (pk-pk)

Station: 5, Sub-Station: 1
Speed range = 4000 - 8000 rpm
probe 1 (x) 0 deg - max amp = 0.021665 at 6000 rpm
probe 2 (y) 0 deg - max amp = 0.021665 at 6000 rpm

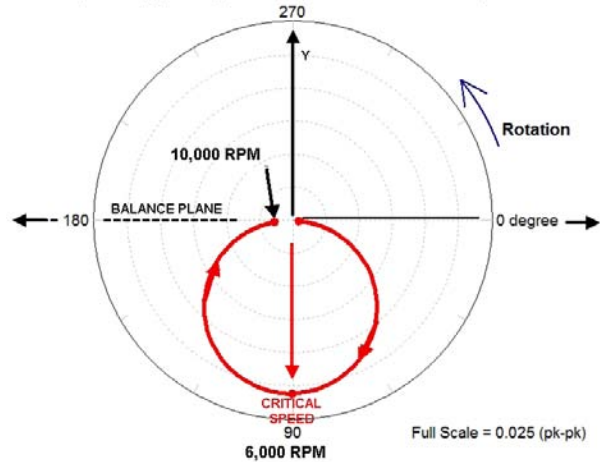


Fig. 15 Polar Plot of Horizontal Motion

Polar Plot of Amplitude And Phase

A useful procedure for viewing the rotor motion is to make a polar plot of the amplitude and phase of the motion. Figure 15 represents the polar plot for the Jeffcott horizontal motion. The plot of the phase angle moves opposite of the direction of rotation. By viewing the polar plot, one may obtain a reasonable ideal of the direction in which to place the correction weight and also the magnitude of the correction weight. For low values of damping, the polar plot is almost a perfect circle. A tangent to the start position and final position shows the plane of the unbalance. The initial trial weight would be placed at 180 deg from the 0 position. In this plot, the peak to peak motion is plotted.

The distance between the initial 0 position and final position represents $2 \times e_u$, the unbalance eccentricity vector. The value of e_u in this case is approximately 0.5 mils. The balance correction is of the order of the unbalance eccentricity times the modal weight is computed to be approximately 2.2 oz-in. At a balance radius of 12 inches this is about 5 grams of correction. For an initial trial weight a lesser amount of several grams would be appropriate.

$$U_s = W_{modal} \times e_u = 276 Lb \times \frac{0.5 \text{ mils}}{1000} \times 16 \text{ oz} / Lb = 2.2 \text{ oz-in}$$

One very important consideration of the operation of a Jeffcott rotor at or near the critical speed is the bearing forces transmitted. At all speeds below the critical speed, the bearing forces transmitted at greater than the rotating load. At the critical speed of 6,000 RPM, the unbalance of 2 oz-in creates a rotating load of 127 lb or about 64 lb/bearing. The actual transmitted bearing force is almost 1600 lb. This is a dynamic transmissibility of 25!

For operation at speeds exceeding the critical speed, bearing forces are greatly reduced.

Transmitted bearing Forces With Jeffcott Rotor-2 Oz-In Unbalance
Bearing no.: 1 at Station: 1
Max Forces = 1592.0 at 6000 rpm

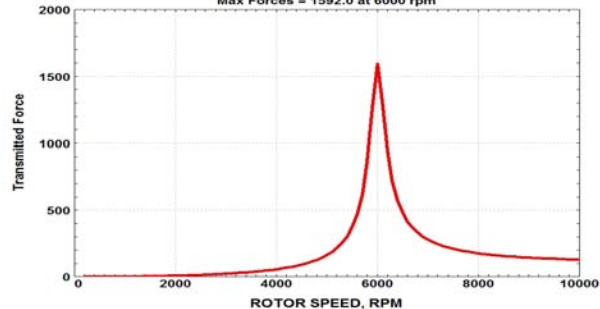


Fig. 16 Bearing Forces Transmitted

Amplitude and Phase of Jeffcott Rotor With Shaft Bow and Unbalance:

The influence of shaft bow may have some unusual effects on the rotor response and also the phase of motion. The effect of shaft bow produced a forced response on the rotor which is constant in magnitude as compared to the effect of unbalance which is a speed squared effect. At the critical speed, the influence coefficients for both effects are identical. Hence at lower speeds, shaft bow has a greater effect, while at speeds above the critical speed, the influence of rotor unbalance predominates. A most interesting effect occurs when the shaft bow is out of phase to the unbalance vector.

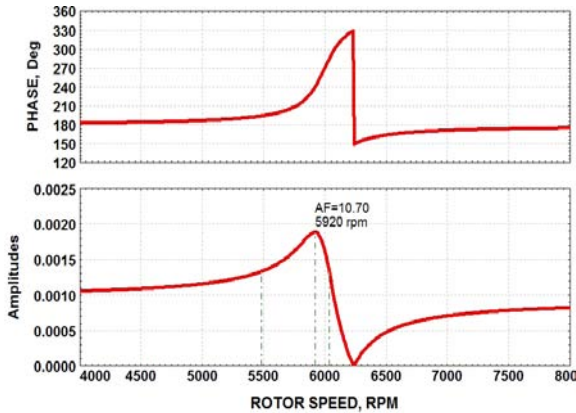


Fig. 17 Bode Plot With Shaft Bow Out of Phase to Rotor Unbalance

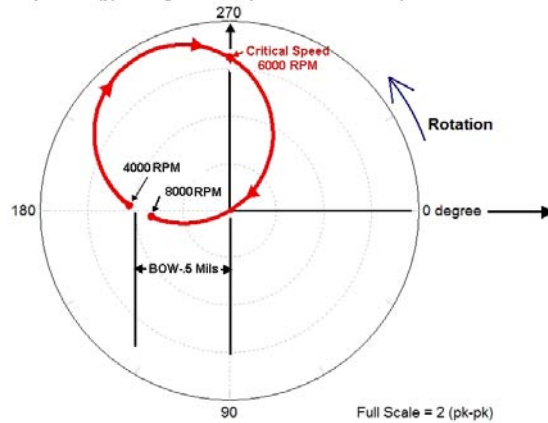


Fig. 18 Polar Plot With Shaft Bow Out of Phase to Rotor Unbalance

In Fig. 17, the shaft bow vector is exactly out of phase with the unbalance vector. The bow vector is .5 mils at 180 deg. At low speeds, the amplitude is 1 mil p-p and is at 180 deg as shown in the upper phase plot. At low speeds, the 2 oz-in unbalance has very little influence on the rotor response. As speed increases, the influence of unbalance grows as speed squared until the rotating unbalance force exactly matches the force generated by the shaft bow. When this occurs, the rotor amplitude goes to zero and the two force systems are balanced. For this example, the balancing speed is around 6250 RPM. As this speed is increased above this balancing speed, the amplitude begins to increase slightly until the rotor is operating or spinning about its mass center. Since the amplitude plot as shown in Fig. 17 is peak to peak motion, the limit of motion for the Jeffcott rotor is $2 \times e_u$. The 2 oz-in causes an unbalance eccentricity of 0.45 mils. Therefore, the maximum p-p high speed runout to be observed will be 0.9 mils as shown in Fig. 17.

To better understand the interaction of shaft bow and unbalance, we need to examine the polar plot of Fig.18. It should be noted, that with a lightly damped system, the polar plot forms very close to a circle. The origin of the circle starts off at 1 mil at the phase angle of 180 deg. The phase change is in the counterclockwise direction opposite to the direction of rotation. From this plot, it is seen that the polar orbit passes through the origin of the coordinate system at 6200 RPM.

General Relationship Between Various Phase Angles And the Keyphasor Probe:

Figure 19 shows the general cross section of the Jeffcott rotor with the arbitrary placements of the unbalance vector and the keyphasor probe. The noncontact probes observe the rotating vector δ which is represented by line O-C. The mass center M is displaced from the axis of rotation by the small eccentricity vector e_u . The angle between the mass center vector and displacement vector is the angle β . The angle actually observed and displayed in the Bode plot will be the angle ϕ since in general, in a real rotor, the mass center will not be aligned with the keyphasor mark.

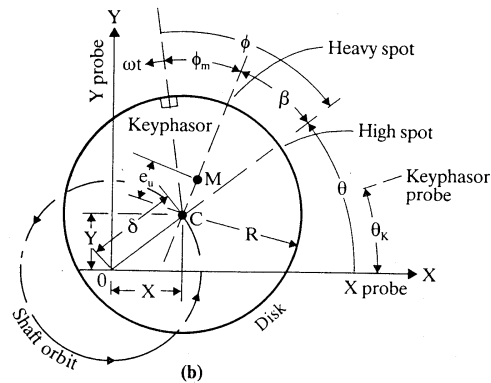


Fig. 19 Deflected Rotor With Keyphasor Probe Showing Mass-Displacement Phase Relationships

Jeffcott Rotor With Coupling Weight:

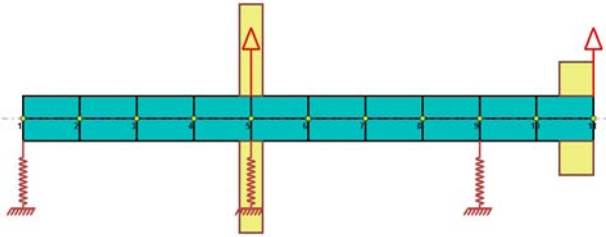


Fig 20 Jeffcott Rotor With Coupling Weight

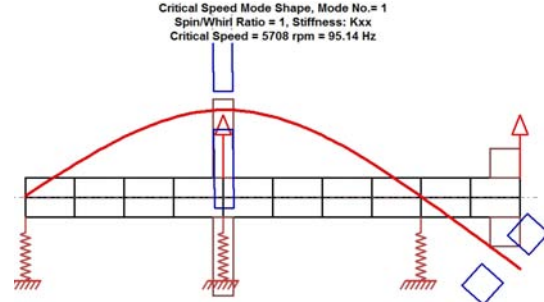


Fig. 21 1ST Mode Jeffcott Rotor With Coupling Weight - $N_{c1} = 5,708$ RPM

Figure 20 represents the Jeffcott rotor with a shaft extension a 20 lb coupling weight attached. The addition of the coupling weight causes a reduction of the critical speed from 6,000 RPM to 5,708 RPM as shown in Fig.21. In Fig. 21, it is seen that the coupling motion is out of phase to the center span disc motion. At higher speeds, a second critical speed at 16,890 RPM will be encountered. This mode is mostly due to the dynamical behavior of the coupling with little motion at the central disk. Large coupling overhangs are to be avoided due to their highly undesirable behavior at elevated speeds.

The coupling location is often used for a trim balancing plane often with unusual phase change results.

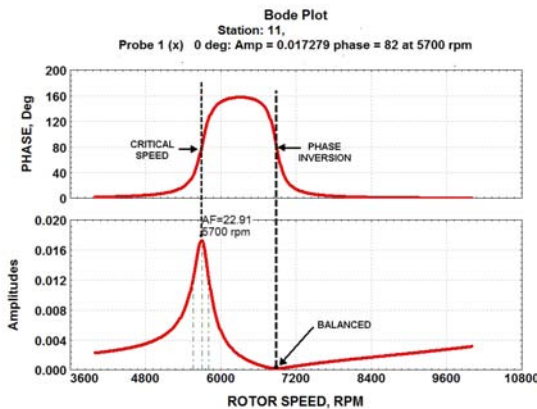


Fig. 22 Coupling Response With 2 Oz-In Ub In Phase With Disc Unbalance

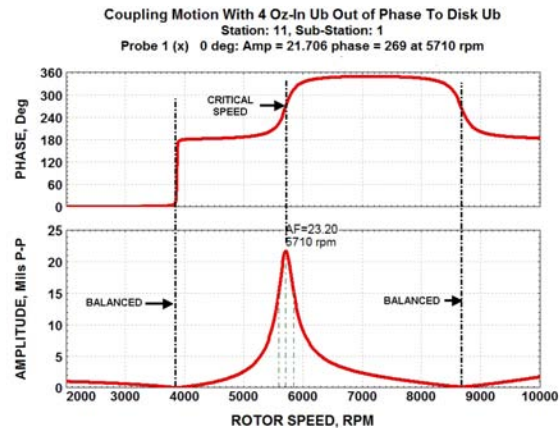


Fig. 23 Coupling Response With 4 Oz-In Ub Out of Phase to Disc Unbalance

Figure 22 shows the coupling end motion with a trim balance weight of 2 oz-in added in-phase to the 2 oz-in unbalance on the center disc. The critical speed is at 5,700 RPM as predicted by the critical speed analysis. The amplification factor observed at the coupling location is approximately 23. As the rotor passes through the critical speed region, there is a phase inversion between the mass unbalance on the disc and the coupling.

This mass inversion leads to an apparent local balancing of the coupling at around 7,000 RPM. The phase angle initially has gone through a 180 deg phase change, which is to be expected for the Jeffcott rotor. The reversal of phase then occurs. After a 90 deg reversal has occurred, we obtain a nodal point with zero motion at the coupling.

This point is sometimes referred to as the “anti resonant” speed and corresponds to a 90 deg phase shift reversal. A similar effect will also be observed with tuned support systems. As the speed is increased above the anti-resonance speed, the coupling amplitude continues to increase. Note that the coupling motion is continuing to increase with no apparent increase or change in the observed phase angle. The reason for this is because the next critical speed with high coupling motion is not encountered until we reach the 16,000 RPM speed range.

Figure 23 shows the coupling motion with 4 oz-in unbalance out of phase to the disk unbalance. The phase behavior for the coupling end is most unusual as there are two observed anti-resonance speeds created. The first is at low speed around 4,000 RPM. Although the amplitude is small, there is a 180 deg phase shift associated with with speed. The second anti-resonance speed is the higher self balancing speed around 8,500 RPM. There also is a corresponding 180 deg phase reversal associated with this speed. Thus it is apparent that when we observe unusual phase shifts and reversals in phase in apparently simple systems, then it might be worthwhile to examine the coupling and its balance condition.

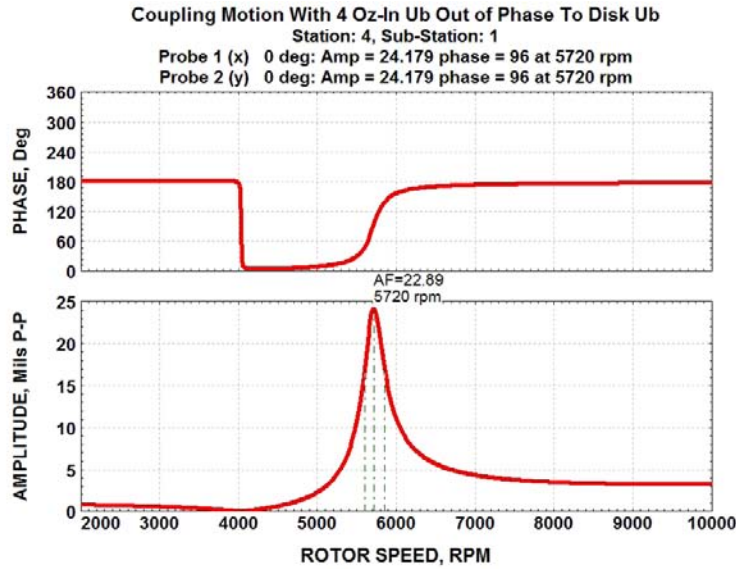


Fig. 24 Motion Near Center Rotor Span With Large 4 Oz-In Coupling Unbalance Out-Of-Phase to the Disk Unbalance

Figure 24 shows the motion near the disk center with the large coupling applied out of phase to the disk unbalance. The behavior appears to be very similar to the expected behavior for the Jeffcott rotor except for the behavior around 4000 RPM. Since the coupling unbalance is out of phase to the disk unbalance, we encounter a balancing or anti-resonance condition at this speed. There is an associated reverse phase shift that occurs corresponding to the nul vibration speed. Although the amplitudes of motion in this low speed range are small, the phase change behavior should not be ignored as this may indicate some external effects to the rotor such as the coupling. Fig. 25 shows that coupling unbalance may lead to high bearing forces at speed.

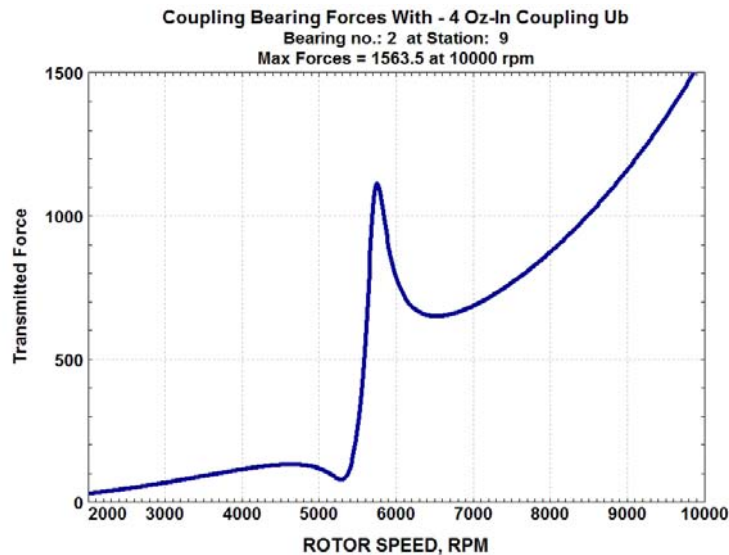


Fig. 25 Coupling End Bearing Forces Transmitted With Large Out-Of-Phase Coupling Unbalance

Amplitude and Phase Behavior For Multimass Rotors:

Figure 26 represents a multimass rotor with the addition of two more disks. Figure 27 represents the first critical speed and mode shape. In general, with multistage compressors and turbines, the first mode shape will be similar in form to the Jeffcott rotor.

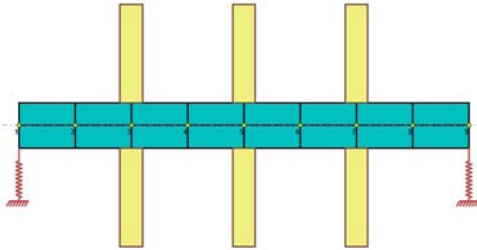


Fig 26 Multimass Rotor in Fluid Film Bearings

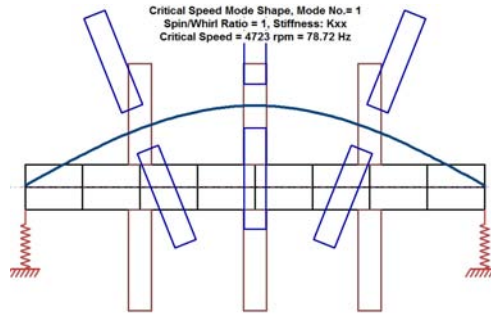


Fig 27 1st Critical Speed Mode For Multimass Rotor

The addition of the additional disks causes a second critical speed to be within the operating speed range of the rotor. Figure 28 represents a critical speed map to include the first two critical speeds as a function of bearing stiffness. It can be seen that for an operating speed range of 10,000 RPM, a second critical speed may easily fall within the operating speed for bearing stiffness values that fall below 300,000 Lb/In.

To avoid this apparent problem, compressor manufacturers would often use highly preloaded tilting pad bearings with bearing stiffnesses exceeding 1.0E6 Lb/In. Although the second critical speed is well removed from the operating speed, this practice would result in very serious rotor aerodynamic instability problems due to reduced modal damping caused by the excessive bearing stiffness.

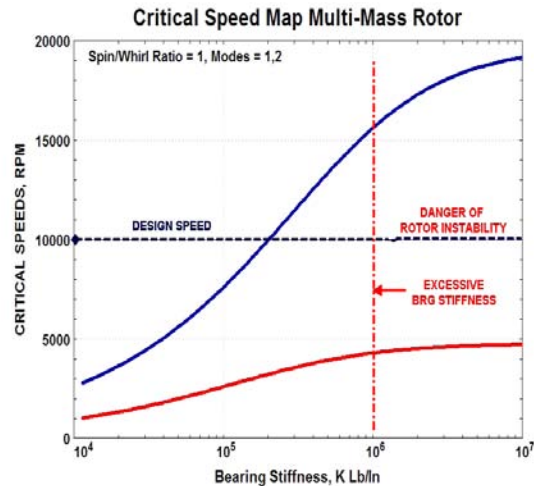


Fig 28 Critical Speed Map For MultiStage Rotor

Tilting Pad Bearing Coefficients:

5 PAD on LOAD ON PAD
 5 Pads, Arc= 60, L/D= 0.5, Cb= 0.005, 2Cb/D=0.0025, m= 0.3, Offset= 0.5, PivAng = 54
 Speed = 6000 rpm
 Load = 200 Lbf
 W/LD = 25 psi
 Vis. = 1E-06 Reysns
 Sb = 0.64
 E/Cb = 0.4908
 Att. = 0.00 deg
 hmin = 2.149 mils
 Pmax = 102.545 psi
 Hp = 1.15708 hp
 Stiffness (Lbf/in)
 3.621E+04 0.000E+00
 0.000E+00 1.401E+05
 Damping (Lbf-s/in)
 1.002E+02 0.000E+00
 0.000E+00 2.100E+02
 Critical Journal Mass
 Stable

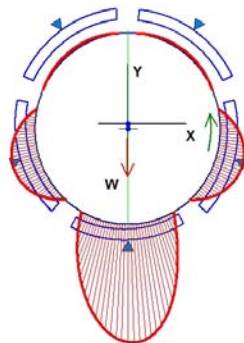


Fig. 29 5 Tilting Pad Brg Coefficients

Tilting Pad Bearing with Rigid Pivot - free to tilt with inertia effect
 4 Pads, Arc= 72, L/D= 0.5, Cb= 0.005, 2Cb/D=0.0025, m= 0.3, Offset= 0.5, PivAng = 45
 Speed = 6000 rpm
 Load = 200 Lbf
 W/LD = 25 psi
 Vis. = 1.01E-06 Reysns
 Sb = 0.6464
 E/Cb = 0.5335
 Att. = 0.00 deg
 hmin = 2.594 mils
 Pmax = 73.0989 psi
 Hp = 1.13745 hp
 Stiffness (Lbf/in)
 8.940E+04 -2.683E+02
 2.683E+02 8.940E+04
 Damping (Lbf-s/in)
 1.644E+02 7.205E-01
 -7.205E-01 1.644E+02
 Critical Journal Mass
 3.357E+004

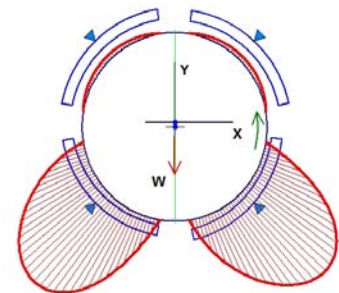


Fig 30 4 Tilting Pad Brg Coefficients

Figure 29 represents a 5 pad bearing with load on pad. The bearing stiffness is asymmetric in the horizontal and vertical directions. Hence the synchronous amplitude and phase measurements will be different for the two directions. The x stiffness $K_{xx} = 36,000$ Lb/in and the y stiffness is $K_{yy} = 140,000$ Lb/in.

The x damping for the 5 pad bearing is $C_{xx} = 100$ Lb-sec/in and the y damping is $C_{yy} = 210$ Lb-sec/in.

Figure 30 shows the corresponding stiffness for a 4 pad bearing configuration with load between pads. In this case, it is seen that the stiffness and damping coefficients for the 4 pad bearing are symmetric in the x and y directions. The values for stiffness are $K_{xx} = K_{yy} = 89,000$ Lb/in and the values for damping are $C_{xx} = C_{yy} = 164$ lb-sec/in. It should be noted that the bearing stiffness and damping coefficients are approximately the average values of the 5 pad bearing configuration. Since the bearing coefficients for the 5 pad bearing are asymmetric, the motion in general will be elliptical in nature. This means that probes stationed at the horizontal and vertical directions will observe different values of amplitude and phase. In contrast, the bearing coefficients for the 4 pad bearing are symmetric. Hence the whirl orbits due to unbalance will be circular in nature. Therefore, the synchronous phase angle changes with speed will be similar in both the horizontal and vertical directions.

Damped Complex Modes With Tilting 5 Pad Bearing Configuration:

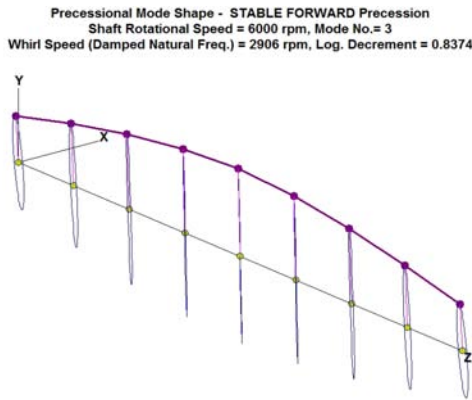


Fig. 31 $N_{1f} = 2,906$ CPM With 5 Pad Brgs,
Log Dec = 0.837 , $A_c = 3.75$

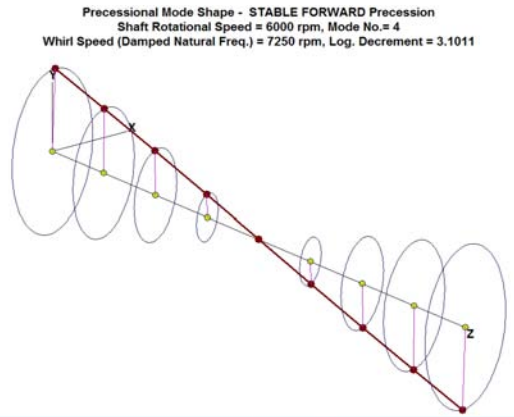


Fig 32 $N_{2f} = 7,250$ CPM With 5 Pad Brgs
Log Dec = 3.11 , $A_c = 1.01$

Unbalance Response Amplitude and Phase With Tilting 5 Pad Bearings:

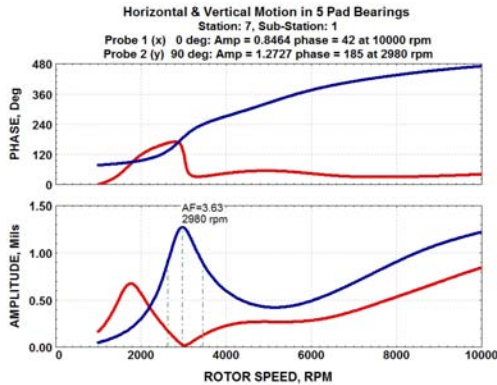


Fig. 33 Horizontal and Vertical Motion at
St 7 With Tilting 5 Pad Bearings

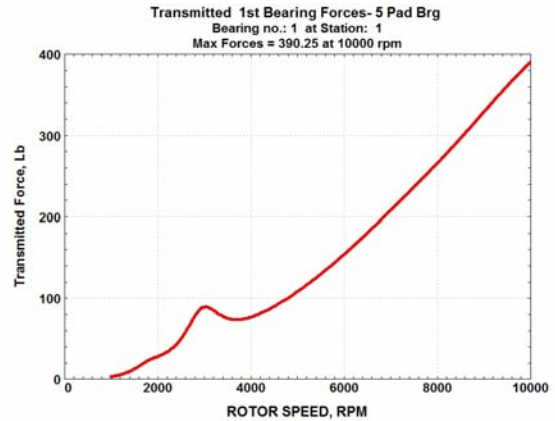


Fig. 34 Bearing Forces Transmitted With 5 Pad
Bearing Configuration

Figure 33 represents the synchronous forced unbalance with the 5 pad bearing configuration. Note that the 1st critical speed will occur at a speed depending upon which probe one is observing. There is a mild critical speed observed in the horizontal direction around 2,000 RPM. The major critical speed will be observed in the vertical direction and this will be at the higher speed of 2,980 RPM. This value corresponds well with the computed damped 1st forward mode of 2,906 CPM. In general, the damped mode frequency will be below or less than the speed of maximum unbalance response. The amplification factor computed by the half power point method is shown to be 3.63 in Fig. 33. Note that the amplification factor calculated from the log decrement as shown in Fig. 31 is given as 3.75. At the 1st major critical speed at 2,980 RPM, the motion is entirely vertical. There is no x motion!

In Fig 33, for the horizontal motion, we see that the amplitude continues to increase above the 3,000 RPM speed range but the phase angle does not. The horizontal phase angle remains relatively constant.

The second damped forward mode as shown in Fig. 32 is a conical mode at a frequency of 7,250 CPM. There does not appear to be any forced response critical speed in this vicinity. The reason for this is because of the high value of the log decrement for this mode. As shown in Fig. 32, the log decrement is 3.11. This gives an amplification factor of 1.01. This means that the mode can not be excited by unbalance. The conical mode is essentially a rigid body motion with large amplitudes of motion at the bearings. In earlier times, compressor manufacturers were fearful of operation on top of a critical speed (some still are). The ability to compute complex damped eigenvalues was not well established. This lead to many improperly designed compressors with 5 pad bearings with excessively tight bearing clearances because of misconceptions on 2nd critical speed operation and the misconceptions on the role of bearing asymmetry on promoting rotor stability.

Damped Complex Modes With Tilting 4 Pad Bearing Configuration:

Figure 35 represents the 1st damped forward mode with 4 pad bearings. The log decrement with the 4 pads is superior to the 5 pad design resulting in a lower amplification factor for the 1st mode. Figure 36 represents the 2nd forward damped mode. Since the log decrement is over 3.14, there is no apparent 2nd critical speed to excite. It is apparent that the 4 pad bearing has superior damping over the 5 pad bearing configuration and will, in general ,have superior stability characteristics.

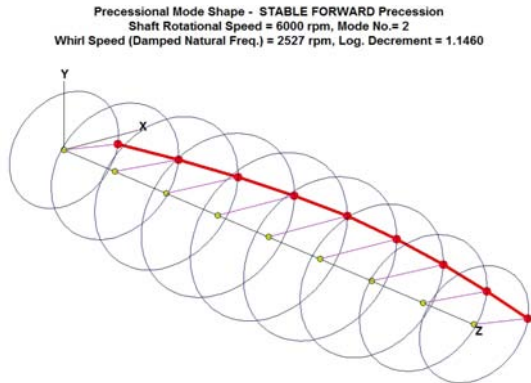


Fig 35 1st Forward Mode at 2527 CPM With 4 Pad Brgs - Log Dec = 1.146 , Ac = 2.74

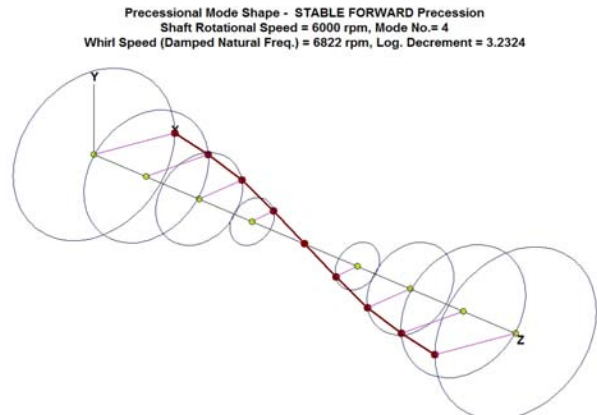


Fig. 36 2nd Forward Mode at 6,822 CPM With 4 Pad Brgs - Log Dec = 3.232

Figure 37 represents the amplitude at the rotor center and at the end bearing with the 4 pad bearings. The center span motion looks like a Jeffcott rotor response with an amplification factor of 2.7. Since there is no second critical speed at 6,800 RPM, the amplitude of motion at the bearing continues to increase with speed.

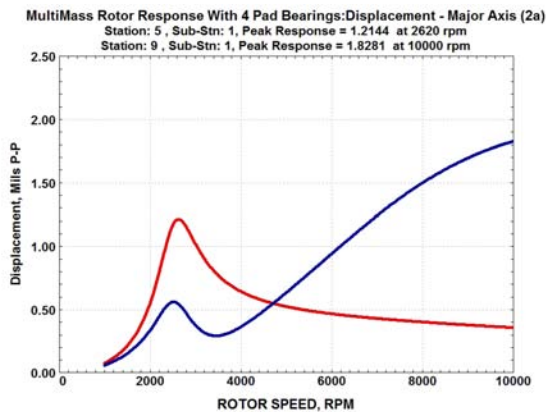


Fig 37 Amplitude At Center and Brg Locations With 4 Pad Brgs

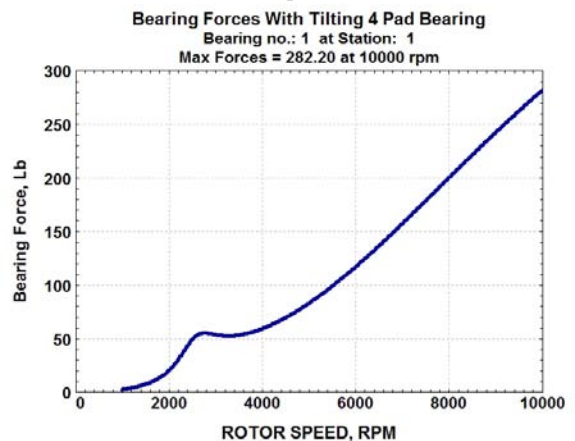
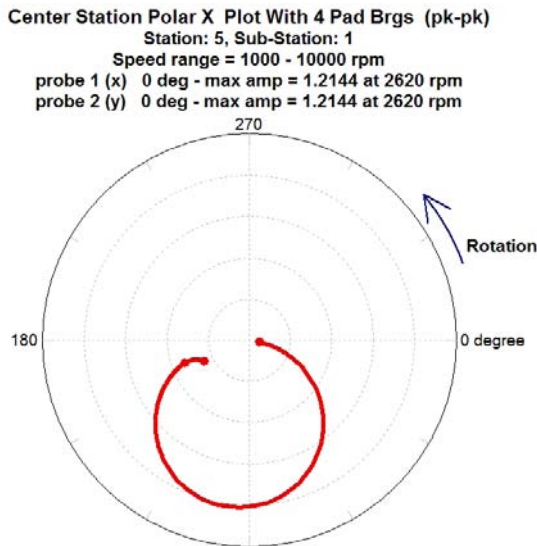


Fig 38 `Bearing Forces Transmitted With 4 Pad Brgs

Figure 38 represents the bearing forces transmitted with the 4 pad bearing configuration. After passing through the 1st critical speed, the bearing forces reduce. Above 3,500 RPM, the bearing forces continue to increase. This is due to the high value of bearing damping which suppresses the second critical speed. Although we do not encounter a second critical, we have the undesirable situation of increasing bearing forces with speed. However, the system behavior with the 4 pad bearings are superior to the response and bearing forces encountered with the 5 pad bearing configuration. Except for the case of heavy turbines where jacking oil is required for liftoff, there is no advantage to the use of the 5 pad bearing arrangement for normal compressor design. This is a mistaken design concept that has persisted for far too long.

Polar Plots Of Rotor Center and Bearing Response With 4 Pad Bearings:

Figure 39 represents the polar plot of the horizontal motion with the 3 planes of unbalance and the rotor supported by the 4 tilting pad bearing configuration. The response at the rotor center appears to be similar to that of the Jeffcott rotor. As we move further away from the center, we pick up the effects of the second mode. Figure 40 shows the polar plot obtained at the first bearing. As the rotor passes through the first critical speed region, the amplitude reaches a minimum around 3,500 RPM with a maximum phase change of 120 deg. The polar plot then forms a small inner loop as the amplitude begins to increase without substantial change in the phase angle. Whenever this is observed at the bearing location, this is an indication that the bearing forces are also increasing.



**Fig. 39 Polar Plot of Center Span X Motion
4 Pad Bearings**

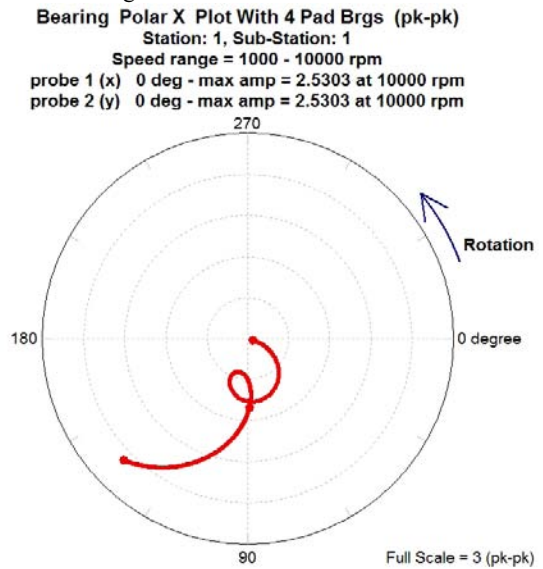


**Fig. 40 Polar Plot of Bearing X Motion
4 Pad Bearings**

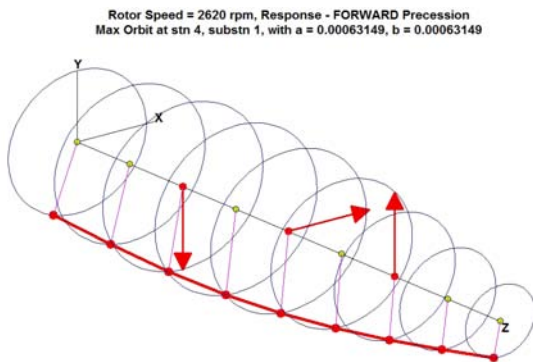


**Fig 41 Rotor Response at 2620 Rpm With
3 Planes of Unbalance- 4 Pad Brgs**

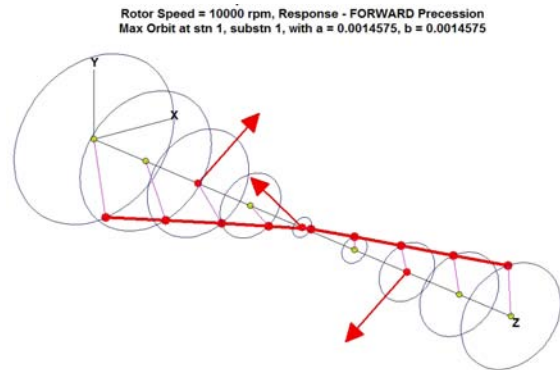


**Fig. 42 Rotor Response at 10,000 RPM With
3 Planes Unbalance - 4 Pad Brgs**

Figure 41 shows the 3 dimensional mode shape at 2620 Rpm. The center plane of unbalance is leading the shaft deflection by 90 deg. Fig. 42 shows the motion at 10,000 RPM. The center motion is a node point at this speed.

Rotor Response With High Preloaded Tilting 4 Pad Bearings:

The 4 Pad bearing configuration as shown in Fig. 30 has a low preload of 0.3 and a large bearing radial clearance C_b of 5 mils. This preload and clearance combination leads to a relatively soft bearing. The rotor has a low amplification factor at the first critical speed and is highly stable from the standpoint of self excited whirl instability with respect to Alford type cross-coupling forces acting on the impellers. However, since all centrifugal compressor manufacturers embed their noncontact probes at or near the bearings, there is the impression that the vibrations are excessive and hence install bearings with higher preloads and tighter bearing clearances.

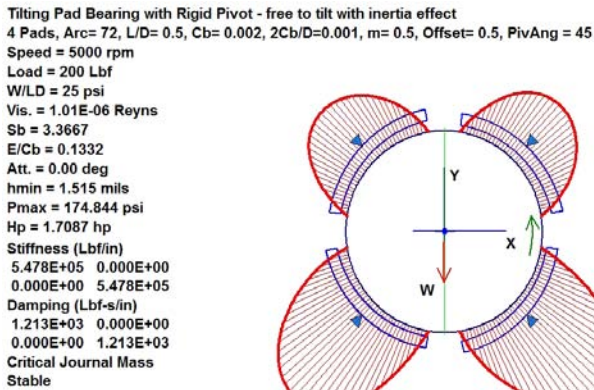


Fig 43 Tilting 4 Pad Brg With Preload $m=0.5$ and Bearing Radial Clearance $C_b = 2$ Mils

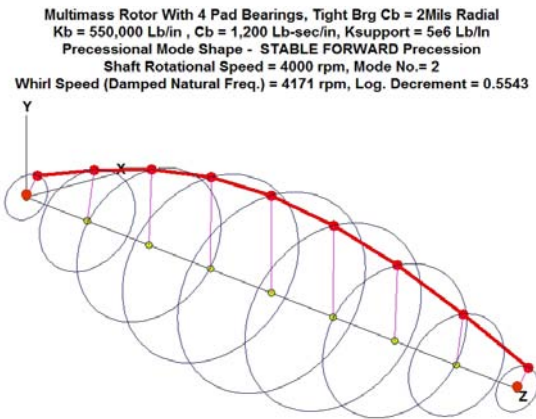


Fig 44 1st Forward Mode At 4117 CPM With 4 Pad Brgs, $C_b = 2$ Mils, $LD = .554$, $Ac=5.67$

Figure 43 represents the bearing coefficients for the 4 pad bearing with the bearing preload increased to $m = 0.5$ and the radial bearing clearance C_b reduced from 5 to 2 mils. This dramatically increases the bearing stiffness and damping coefficients by causing the upper pads to be active. Figure 44 represents the resulting 1st forward mode with the stiffened bearings. Note, however, the rotor log decrement has been reduced in half.

Influence of Flexibility and Mass on Rotor Response:

In actuality, one can not obtain the full stiffness and damping predicted by a tilting pad bearing program assuming rigid pivots. The influence of pivot flexibility and foundation flexibility causes a reduction of stiffness, but more importantly, it can lead to a drastic reduction of damping.

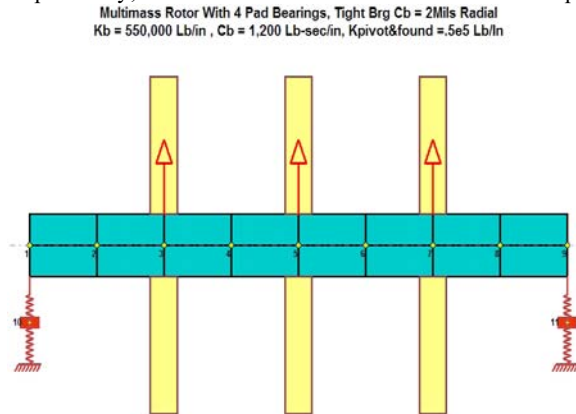


Fig 44 3 Mass Rotor With Flexible Supports

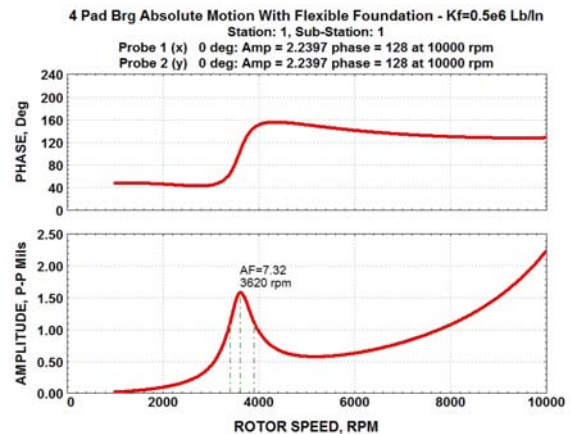


Fig. 45 Amplitude and Phase at 1st Bearing

Figure 44 represents the 3 mass rotor mounted on flexible supports. The support flexibility is assumed to be $.5e6$ Lb/in. The introduction of support flexibility reduces the first critical speed, but more importantly, the foundation flexibility can cause a dramatic reduction in the effective damping. Figure 45 represents the amplitude and phase at the first

bearing. Note that the computed amplification factor based on the half power method is 7.32. This is in comparison to the damped eigenvalue analysis of 5.67 based on the bearings in rigid supports. The damping values of 1200 Lb-sec/in are not obtained in an actual situation.

The introduction of pivot flexibility and foundation flexibility can cause a 50% or higher reduction in the effective damping in a tilting pad bearing configuration.

Rotor 3 Dimensional Modes Shapes and Bearing Polar Plots With Flexible Supports:

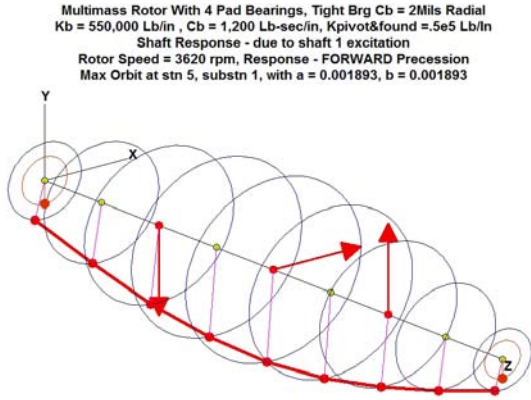


Fig. 46 3 D Mode Shape at 3620 RPM With Flexible Support Kf=.5e6 Lb/In

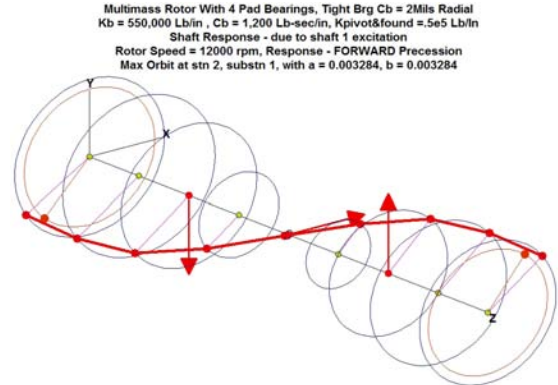


Fig. 47 3 D Mode Shape at 12,000 RPM With Flexible Support Kf=.5e6 Lb/In

Figure 46 represents the rotor unbalance response at 3,620 RPM which is the critical speed with introduction of the flexible supports. The center station unbalance at station 5 is leading the center motion by 90 deg. Figure 47 shows the rotor motion at the higher speed of 12,000 RPM. At this higher speed, the center span motion becomes a node point and the unbalance at station 5 has no influence on the shaft motion at this elevated speed above the first critical speed. The bearing motions are out of phase to each other.

4 Pad Brg Absolute Polar Plot With - Kf = 0.5e6 Lb/In (pk-pk)
 Station: 1, Sub-Station: 1
 Speed range = 1000 - 12000 rpm
 probe 1 (x) 0 deg - max amp = 0.0064511 at 12000 rpm
 probe 2 (y) 0 deg - max amp = 0.0064511 at 12000 rpm

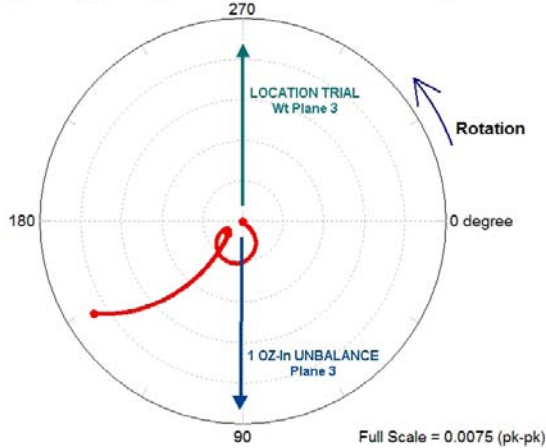


Fig. 48 Polar Plot of 1st Bearing Motion From 1,000 RPM to 12,000 RPM

4 Pad Brg #2 Polar Plot With Kf = 0.5e6 Lb/In (pk-pk)
 Station: 9, Sub-Station: 1
 Speed range = 1000 - 12000 rpm
 probe 1 (x) 0 deg - max amp = 5.8801 at 12000 rpm
 probe 2 (y) 0 deg - max amp = 5.8801 at 12000 rpm

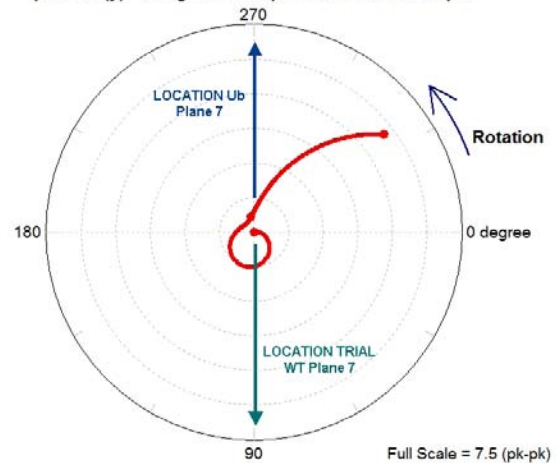


Fig. 49 Polar Plot of 2nd Bearing Motion From 1,000 RPM to 12,000 RPM

Figure 48 represents the polar plot for bearing station 1. The small inner circle represents the passage through the first critical speed. As the rotor speed exceeds 140% of the first critical speed, which is around 5,000 RPM, the polar plot moves out at a phase angle of 120 deg and slightly increases in phase. The phase displacement above

5,000 RPM lags the unbalance at 90 deg at station 3. Since the second critical speed is still well above the maximum speed of 12,000 RPM, the polar plot moves out radially with little phase change. Figure 49 represents the polar plot at the second bearing. The 2 unbalances at stations 3 and 7 act as a couple unbalance. Hence to properly balance the rotor above 5,000 RPM, a two plane balance procedure must be used.

Bifurcated or Split Critical Speeds With Tuned Rotor-Supports:

In the previous case, the introduction of support flexibility causes a reduction of the critical speed and a significant reduction in the effective bearing damping. When foundation mass is introduced, an interesting effect can occur if the foundation mass and support natural frequency are close to the rotor critical speed. The foundation interacts with the rotor to form a tuned resonance condition in which a bifurcated or split critical speed is created.

Figure 50 represents the 1st split critical speed with foundation or support mass of 500 Lb included under the first bearing. The total effective support stiffness is taken as 0.25e6 Lb/in. This creates a foundation resonance around 4100 CPM. Since this frequency is close to the original critical speed with the tilting pad bearings on a rigid foundation, the critical speed mode is bifurcated into two families. These two frequencies occur above and below the original critical speed. In Fig. 50, the foundation and 1st bearing motion are in phase. Since the relative motion between the bearing and support are in phase, the effective damping is reduced. This causes the rotor critical speed amplification factor to increase to 18 as predicted from the damped eigenvalue analysis. Figure 51 represents the upper branch of the split critical speed mode. In this case, the foundation and bearing are out of phase and hence the effective damping is increased. For this mode, the amplification factor is predicted to be 8.8. Therefore the lower branch of the split critical speed may be very difficult to balance because of the reduced damping. This condition can occur with a soft footing under a machine.

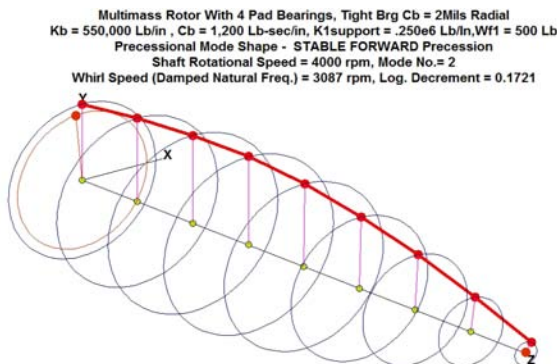


Fig. 50 1st Split Critical Speed At 3087 RPM
Wf=500 Lb, Kf=.25e6Lb/In , LD=.172, Ac= 18

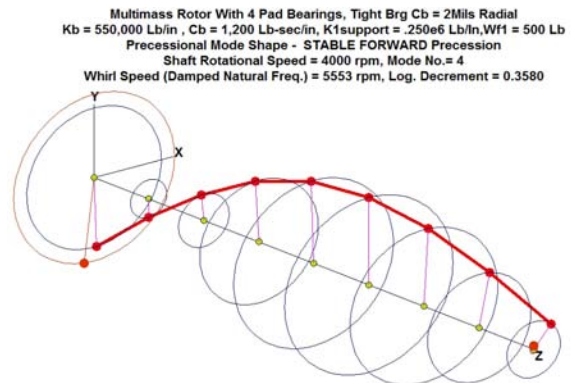


Fig. 51 2nd Split Critical Speed At 5553 RPM
Wf=500 Lb, Kf=.25e6Lb/In , LD=.358, Ac= 8.8

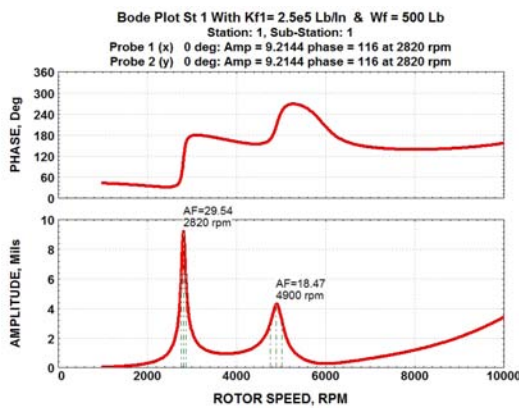


Fig 52 Amplitude and Phase At 1st Bearing
Wf = 500 Lb , Kf=.25e6 Lb/In

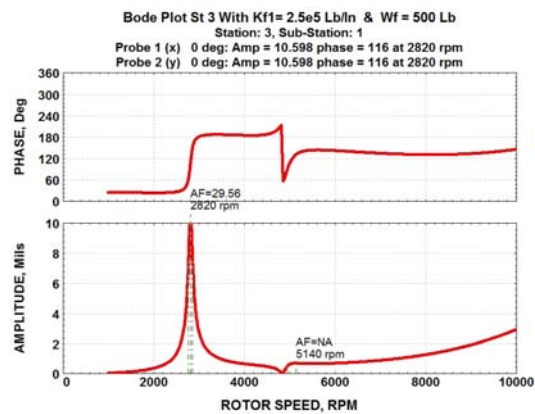


Fig 53 Amplitude and Phase At Station 3
Wf = 500 Lb , Kf=.25e6 Lb/In

Figure 52 represents the motion at the first bearing and Fig. 53 shows the motion at the rotor quarter span.

Note that in both Figs. 52 and 53, the first branch of the bifurcated critical speed has an amplification factor as computed by the half power point method of over 29. This condition would make this mode most difficult to balance. This situation has been encountered with aircraft engine rotor-casing interactions, industrial gas turbines with flexible hot end supports, and with exciters with damaged grouting. The exciters become almost impossible to balance until the foundation grouting is repaired. In Fig. 53, note that there is an antiresonance speed at station 3 at 5140 RPM with null vibrations. Figure 54 shows the motion at the shaft center. Note the high amplification factor of 29.

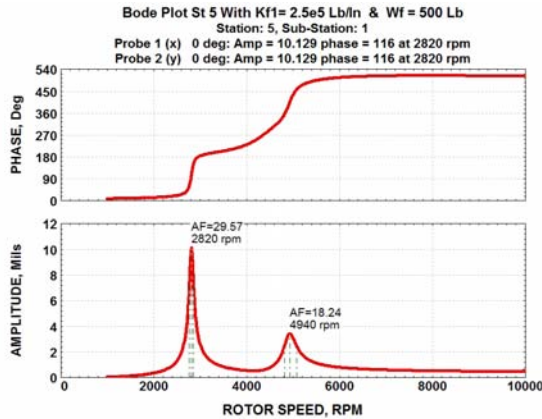


Fig 54 Amplitude and Phase at Rotor Center
 $Wf = 500$ Lb , $Kf = .25e6$ Lb/in

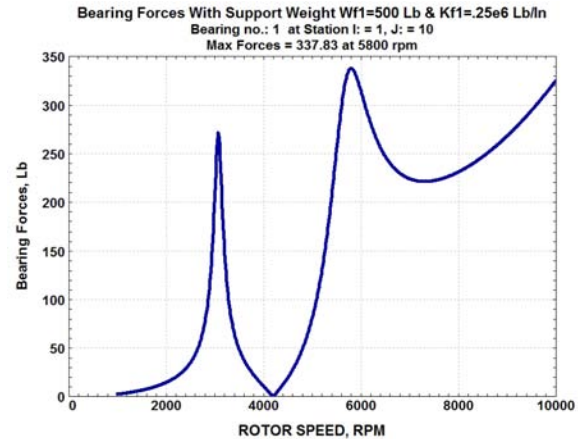


Fig. 55 Bearing Forces Transmitted With Resonant Support Condition

The high amplification factor encountered at the rotor center span could lead to seal rubs. Figure 55 represents the forces transmitted at the first bearing with the resonant support condition under bearing 1.

Discussion and Conclusions:

The knowledge of the behavior of the synchronous unbalanced and forced response phase changes with speed for rotating machinery can be an important tool in the balancing and diagnostics of many field problems. Unfortunately a large number of rotors have not been designed to properly incorporate adequate instrumentation to monitor vibration and phase of motion. This has caused great difficulties with correcting vibration problems encountered with such varied equipment as the space shuttle engines, aircraft gas turbines, large turbine generators, and centrifugal compressors and large industrial fans.

The typical phase change of 0 to 180 deg associated with the simple Jeffcott rotor is well understood. The complication in interpretation occurs when we encounter more complex multimass models with such diverse effects as overhung disks, shaft bow and mass foundation effects. It is often advisable to have a record of the initial amplitude and phase for various probes on initial installation of a machine. Significant changes of phase during the operation of the rotor over time can be indications for maintenance. Without phase readings, single and particularly multi plane balancing is virtually impossible. Also, by having a proper time mark signal, one can generate Bode and Nyquist plots of the rotor motion. For aircraft engines, two timing reference signals are required for two spool rotors to separate the high rotor from the low speed rotor. A great deal of acquired aircraft engine vibration data has often proved to be of limited value due to the absence of an adequate reference signal for synchronous tracking. This is particularly important when squeeze film dampers are employed with aircraft engines. When the nonlinear dampers become overloaded, we see the effect by the change in phase. In a normal rotor, a change in phase with increased unbalance is not pronounced if the rotor is operating in a linear range. This is not the case with squeeze film dampers as they become highly nonlinear with increases in unbalance. Synchronous phase monitoring for aircraft engines is extremely important.

A great deal of understanding of the of the relationships between amplitude and phase for multimass rotor system may be gained by the modeling of the system with the inclusion of such various effects such as skewed disks, misalignment, shaft bow as well as the inclusion of radial unbalance encountered with rotating equipment. In this presentation, some of these basic effects are included. Careful inspection of the phase behavior over a speed range for various probes can significantly improve our understanding of the dynamical behavior of rotating machinery.